Precision measurements of a simple chaotic circuit

Ken Kiers[a] and Dory Schmidt[b]
Department of Physics, Taylor University, Upland, Indiana 46989

J. C. Sprott[c]
Department of Physics, University of Wisconsin, Madison, Wisconsin 53706

(Received 10 June 2003; accepted 27 August 2003)

We describe a simple nonlinear electrical circuit that can be used to study chaotic phenomena. The circuit employs simple electronic elements such as diodes, resistors, and operational amplifiers, and is easy to construct. A novel feature of the circuit is its use of an almost ideal nonlinear element, which is straightforward to model theoretically and leads to excellent agreement between experiment and theory. For example, comparisons of bifurcation points and power spectra give agreement to within 1%. The circuit yields a broad range of behavior and is well suited for qualitative demonstrations and as a serious research tool.
[DOI: 10.1119/1.1621031]

I. INTRODUCTION

The study of nonlinear systems and chaos provides a fascinating gateway into the world of research for students. With the growing use of nonlinear analysis techniques in many areas of science, it also is becoming increasingly important to provide undergraduate students with a good introduction to nonlinear systems. Undergraduate chaos experiments that are available commercially tend either to be relatively expensive or to be somewhat qualitative in nature. Many articles have been published over the past 15 years regarding chaotic behavior in systems ranging from a bouncing ball to various electronic circuits.[1–8] In many of these articles the authors have made clever use of low cost or readily available equipment to illustrate well-known aspects and analytical techniques associated with chaos, such as bifurcation diagrams, periodic and chaotic attractors, return maps and Poincaré sections.

Nonlinear electronic circuits provide an excellent tool for the study of chaotic behavior. Some of these circuits treat time as a discrete variable, employing sample-and-hold subcircuits and analog multipliers to model iterated maps such as the logistic map.[1] Continuous-time flows are somewhat easier to model electronically. One of the best-known chaotic circuits of this latter type is Chua's circuit.[9–11] The original version of this circuit contains an inductor (making it difficult to model and to scale to different frequencies), but inductorless versions of Chua's circuit have also been described.[12–14] Recent work has highlighted several new chaotic circuits that are very simple to construct and analyze.[15,16] These circuits correspond to simple third-order differential equations, are easy to scale to different frequencies, and contain only simple electronic elements such as diodes, operational amplifiers (op amps), and resistors. Furthermore, with slight modifications, they hold the potential for very precise comparisons between theory and experiment.[17] The differential equations corresponding to these circuits are among the simplest third-order differential equations that lead to chaotic behavior.[18–22] As noted in Refs. 16 and 17, several of these circuits may be grouped together and regarded as an analog computer for the precise experimental study of chaotic phenomena. Some possible uses of these circuits involve studies of synchronization[23] and secure communication.[24] Furthermore, several such circuits could in principle be linked together to investigate higher-dimensional chaos.

One class of simple circuits that leads to chaotic behavior is described by the following third-order differential equation,[17]

$$\dddot{x} = -A\ddot{x} - \dot{x} + D(x) - \alpha, \tag{1}$$

where x represents the voltage at a particular node in the corresponding circuit. In Eq. (1) A and α are constants, the dots denote derivatives with respect to a dimensionless time, and $D(x)$ is a nonlinear function that characterizes the nonlinearity in the circuit.

In this paper we describe an investigation of a new circuit belonging to the class of circuits described by Eq. (1). The nonlinearity in the circuit models a function proportional to $\min(x,0)$. The circuit is similar to the one described in Ref. 15, but uses a more precise implementation of the nonlinearity.[25] The increase in precision allows for a detailed comparison between theory and experiment. Such comparisons yield agreement to within 1% for quantities such as bifurcation points. The data taken from the circuit also can be used in a variety of ways to illustrate many aspects of chaotic and periodic behavior.

The paper is structured as follows. In Sec. II we describe the circuit and provide several technical details. Section III contains the experimental results and compares these to theoretical expectations. Section IV offers some concluding remarks.

II. CIRCUIT

A. General remarks

Figure 1 shows a schematic diagram of the circuit used to model Eq. (1). The circuit has a modular design and may, with small changes, be used to study any of several different chaotic systems, each corresponding to a different nonlinear function $D(x)$.[16,17] The variable resistor R_v acts as a control parameter, moving the system in and out of chaos, and the input voltage V_0 may be either positive or negative.[26] All unlabeled resistors (capacitors) have the same nominal resistance R (capacitance C). The box labeled $D(x)$ in Fig. 1 represents the nonlinearity in the circuit, which is necessary

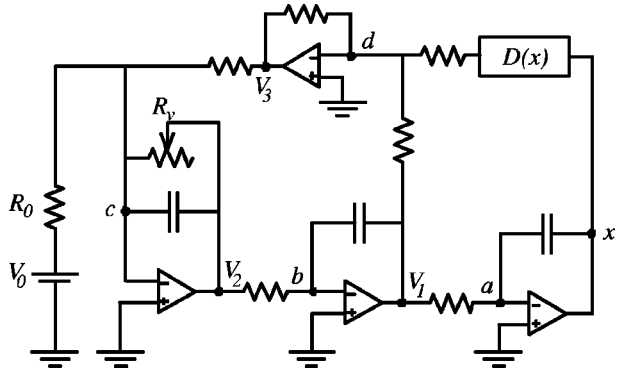

Fig. 1. Schematic diagram of the circuit described by Eq. (6). The box labeled $D(x)$ represents a nonlinear subcircuit. Nominal values for the unlabeled resistors and capacitors are $R=47\ \mathrm{k}\Omega$ and $C=1\ \mu\mathrm{F}$. Approximate values for the input voltage and resistor are $V_0=0.250$ V and $R_0=157\ \mathrm{k}\Omega$. Also, $V_1=-\dot{x}$ and $V_2=\ddot{x}$. The experiment employs dual LMC6062 operational amplifiers, chosen for their high input impedance. Power supplies for the operational amplifiers are tied capacitively to ground to reduce the effects of noise on the circuit.

for the circuit to exhibit chaotic behavior. The voltage at the output of the box (on the left) is related to that at its input by the functional relation $V_{\mathrm{out}}=D(V_{\mathrm{in}})$.

The circuit in Fig. 1 contains three successive inverting integrators with outputs at the nodes labeled V_2, V_1, and x, as well as a summing amplifier with its output at V_3. If we use Kirchhoff's rules at nodes a-d (along with the "golden rules" for op amps[27]), we obtain the following relations among the voltages:[28]

$$V_1=-RC\frac{dx}{dt}=-\dot{x}, \tag{2}$$

$$V_2=-RC\frac{dV_1}{dt}=\ddot{x}, \tag{3}$$

$$RC\frac{dV_2}{dt}=-\left(\frac{R}{R_v}\right)V_2-\left(\frac{R}{R_0}\right)V_0-V_3, \tag{4}$$

$$V_3=-V_1-D(x), \tag{5}$$

where the dots denote derivatives with respect to the dimensionless variable $\tilde{t}=t/(RC)$. The substitution of Eqs. (2), (3), and (5) into Eq. (4) yields

$$\dddot{x}=-\left(\frac{R}{R_v}\right)\ddot{x}-\dot{x}+D(x)-\left(\frac{R}{R_0}\right)V_0. \tag{6}$$

Equation (6) may be compared with Eq. (1). It is straightforward to generalize Eq. (6) to the case where the resistors and capacitors differ slightly from their nominal values.

In Ref. 17 the nonlinearity in the circuit was taken to have the form of an absolute value, $D(x)=|x|$. The solutions of the differential equation corresponding to this form become unbounded when R_v exceeds a certain threshold. In the circuit itself, such unbounded solutions manifest themselves through saturated op amps, making the circuit somewhat difficult to work with. In particular, it was found that certain power supplies to the circuit had to be turned on in a specific order and in quick succession or the circuit would saturate. This instability manifested itself for all values of R_v, not just those beyond the threshold.

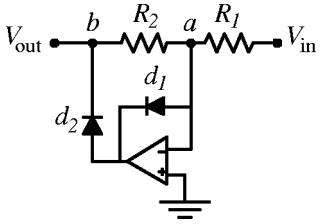

Fig. 2. Schematic diagram of the subcircuit in the box in Fig. 1. The relation between the output and input voltages is given by $V_{\mathrm{out}}=D(V_{\mathrm{in}})=-(R_2/R_1)\min(V_{\mathrm{in}},0)$.

In the present work we employ a different nonlinear subcircuit than in Ref. 17. The nonlinearity used here models the function $D(x)=-6\min(x,0)$ and does not lead to unbounded solutions. The resulting circuit is generally much more stable to work with, making it ideal for use with undergraduate students and for other applications.

Figure 2 shows the nonlinear subcircuit used in this work to model the function $D(x)$ noted above. Slight variations of this circuit[27] are used widely in various electronic applications such as AC voltmeters. To show that the circuit yields the desired functional form, we use the Shockley equation to model the I–V curves for the diodes,

$$I_D=I_S(e^{\alpha V_D}-1), \tag{7}$$

where I_D and V_D represent the current through and voltage across each diode, respectively. For the BAV20 silicon diodes that we use, the reverse bias current I_S is of order a few nA and α is of order $20\ \mathrm{V}^{-1}$. If we employ Kirchhoff's rules at nodes a and b in Fig. 2, we obtain the following transcendental equation relating the input and output voltages in Fig. 2:[29]

$$V_{\mathrm{out}}+\frac{1}{\alpha_2}\ln\left[1+\frac{V_{\mathrm{out}}}{I_{S_2}R_2}\right]=-\frac{1}{\alpha_1}\ln\left[1+\frac{1}{I_{S_1}}\left(\frac{V_{\mathrm{in}}}{R_1}+\frac{V_{\mathrm{out}}}{R_2}\right)\right]. \tag{8}$$

We take $\alpha_1\sim\alpha_2\sim 20\ \mathrm{V}^{-1}$, $I_{S_1}\sim I_{S_2}\sim 3$ nA and resistances of the order 10 kΩ and find that the solution of Eq. (8) is very well represented by the approximate expression

$$V_{\mathrm{out}}=D(V_{\mathrm{in}})=-\left(\frac{R_2}{R_1}\right)\min(V_{\mathrm{in}},0). \tag{9}$$

In the experiment we choose R_1 and R_2 such that $R_2/R_1\approx 6$. In this case the exact solution of Eq. (8) gives voltages of order -10^{-4} V (instead of zero) for positive input voltages. For negative input voltages the exact solution of Eq. (8) differs from the approximation in Eq. (9) by an amount of order $-I_SR_2\sim -2\times 10^{-4}$ V. This amount would yield a 0.3% correction when $V_{\mathrm{in}}=-0.01$ V and a 0.03% correction when $V_{\mathrm{in}}=-0.1$ V. Figure 3 shows an experimental measurement of $D(x)$ as a function of x, with the fit in Eq. (9) superimposed on the data, demonstrating that Eq. (9) models the subcircuit quite well.

One interesting feature that we have observed with the subcircuit is that extremely intense light tends to decrease the output voltage somewhat. (The casing on the diodes is evidently not completely opaque.) No significant effects were observed with normal ambient room light.

The important point expressed in Eq. (9) and the ensuing discussion is that the op amps in Fig. 2 drive the diodes in

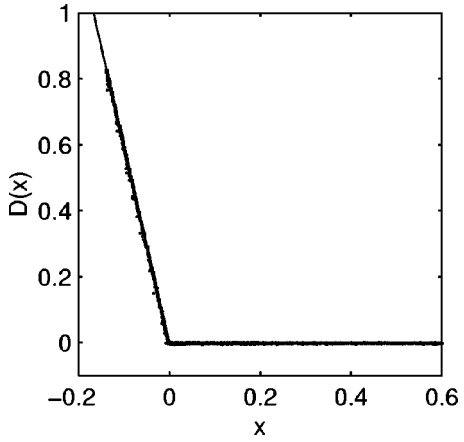

Fig. 3. Experimental measurement of the function $D(x)$ for the nonlinear subcircuit shown in Fig. 2. The superimposed line shows the function defined in Eq. (9). Both x and $D(x)$ are in volts.

such a way that the circuit becomes quite insensitive to the particular characteristics of the diodes themselves, that is, to a very good approximation the solution of Eq. (8) does not depend on α or I_S. A related but slightly simpler version of the circuit in Figs. 1 and 2 employs a bare diode to model the function $\min(x,0)$.[15] A detailed comparison between theory and experiment in that case involves the solution of a differential equation similar to Eq. (6), but with a function $D(x)$ that contains a gradual "knee" rather than a sharp discontinuity in slope. The numerical results depend very sensitively on the exact shape of the knee, so that one must perform a very careful measurement of the diode's $I-V$ curve, and then solve a transcendental equation to determine $D(x)$ accurately.[30] In contrast, the nonlinearity in the present circuit is very well described by the simple piecewise linear function in Eq. (9), which requires no special handling and yields a very accurate representation of the experimental results.

B. Technical details

A few details have been omitted from Fig. 1 for the sake of clarity. In the first place, the circuit is "floated" at a false ground of approximately 0.725 V to accommodate various digital elements in the circuit that were added to collect a time series record of the signal. (These digital elements require voltages to be in the range 0–5 V.) Furthermore, the variable resistor shown in Fig. 1 is actually composed of a 46.3 kΩ fixed resistor in series with eight 256-step DS1803 digital potentiometers (each of nominal resistance $\sim 10\ \mathrm{k}\Omega$). Also omitted from Fig. 1 are simple amplification circuits at the nodes corresponding to x and $-\dot{x}$, which are used to make more efficient use of the 0–5 V range available for analog-to-digital (A/D) measurements.

The digital potentiometers and fixed resistor that comprise R_v in Fig. 1 yield approximately 2000-step resolution over the range from about 50 kΩ to about 130 kΩ. This resolution allows for a very detailed bifurcation plot (see Fig. 4) and also lets the user find very narrow windows of periodicity within bands of chaotic behavior. The digital potentiometers are mildly nonlinear devices in the sense that the resistance of a given potentiometer depends on the voltages at its low and wiper leads. To minimize the effect of this nonlinearity, we calibrate the potentiometers near 0.725 V, the floating ground for the experiment. The potentiometers themselves are controlled digitally by a PIC16773 microcontroller, which also is used to measure the voltages at the nodes corresponding to x and $-\dot{x}$. These voltage measurements are made at a frequency of 166.7 Hz and are stored temporarily on an AT24C256 EEPROM before being transferred serially to a personal computer to be written to a file. Data collection over the entire range of interest takes approximately 12 hours. At present, the limiting factor is the time required to store data on the EEPROM. Modifications are currently planned that will significantly improve this aspect of the experiment.[31]

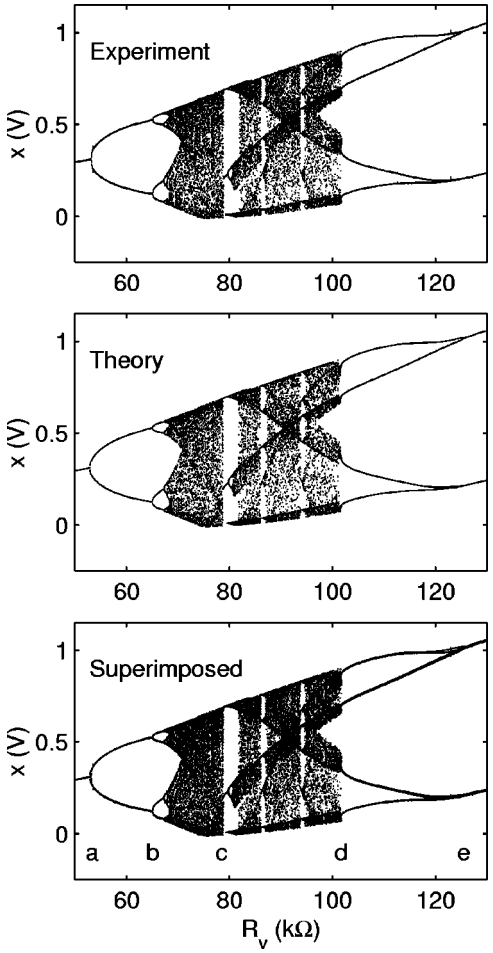

Fig. 4. Experimental, theoretical, and superimposed bifurcation plots for the circuit in Figs. 1 and 2.

III. RESULTS

A. Bifurcation plot

Figure 4 shows experimental and theoretical plots of local maxima of x as a function of R_v. For $R_v \lesssim 53\ \mathrm{k}\Omega$ the voltage varies periodically, with a single maximum occurring near 0.3 V. Near 53 kΩ there is a bifurcation to a period-two wave form. In this case the signal goes through two local maxima before repeating. The signal continues to follow a period-doubling route to chaos as R_v is increased, finally becoming chaotic near 68 kΩ. In chaotic regions the signal never repeats itself, that is, the period is infinite. Also evident in the plots are several windows of periodicity between

Table I. Comparison of theoretical and experimental bifurcation points. The labels a–e are indicated in the bottom plot in Fig. 4.

	Expt. (kΩ)	Theory (kΩ)	Diff. (kΩ)	Diff. (%)
a	53.2	52.9	0.3	0.6
b	65.0	65.0	0.0	0.0
c	78.8	78.7	0.1	0.1
d	101.7	101.7	0.0	0.0
e	125.2	125.5	−0.3	−0.2

bands of chaos. Most of the experimentally observed periodic windows are quite narrow, and can include high-period orbits. (See, for example, the period-10 orbit in Fig. 7, which comes from a periodic window of width 0.3 kΩ near $R_v = 98.2\ \mathrm{k}\Omega$.)

The top plot in Fig. 4 shows the experimental maxima. To reduce the effects of noise on this plot, a cubic polynomial is fit to points surrounding possible maxima. Spurious maxima are removed using various cuts. The fitting procedure generally works very well, but tends to underestimate maxima by up to about 6 mV. The middle plot shows the theoretical bifurcation plot obtained by solving Eq. (6) with the nonlinearity in Eq. (9). The numerical solution is obtained using a fourth-order Runge–Kutta algorithm with a fixed step size corresponding to 0.125 ms. Measured (rather than nominal) values for the resistors and capacitors are used in the numerical work. The bottom plot shows the experimental and theoretical plots superimposed and demonstrates the excellent agreement between the two plots. This agreement also is shown in Table I, which compares the locations of several bifurcation points. The bifurcation points all agree to within 1%. The excellent agreement between theory and experiment is due in large part to the nearly ideal behavior of the nonlinear subcircuit. If a single diode is used to approximate the function in Eq. (9), the agreement between theory and experiment is noticeably poorer (even if one attempts to model the $I-V$ characteristics of the diode carefully.) Figure 5 shows an expanded view of a section of the experimental bifurcation plot shown in Fig. 4, showing the fine detail obtained in the experiment.

B. Power spectral densities and phase portraits

Figure 6 contains several experimental power spectra and illustrates the period-doubling route to chaos followed by the system as R_v is increased from approximately 51 kΩ to 72 kΩ. In each case the results are obtained from an 8192-point fast Fourier transform (FFT) of the corresponding experimental x values.[32] The uppermost plot shows an example of period-one behavior and contains a strong peak at the dominant frequency of approximately 3.1 Hz. The harmonic peaks occurring at integer multiples of the dominant frequency indicate, as would be expected, that the oscillations are not perfectly sinusoidal. A strong peak near 3 Hz is evident in each of the other plots as well, although the peak moves to higher frequencies as R_v increases. The period-one case also contains a theoretical curve for comparison.[33] The agreement between theory and experiment is excellent, with the positions of the peaks agreeing to within one percent. This level of agreement between theory and experiment is found for other values of R_v as well. The second plot in Fig. 6 shows an example of period-two behavior. In this case the oscillating voltage (shown in the inset) passes through two different maxima before repeating. The spectral density plot contains a new peak at half the dominant frequency, illustrating the fact that period doubling is equivalent to frequency halving. The trend is continued in the third plot, which shows an example of a period-four case. The bottom plot shows the power spectrum for a chaotic case. Despite the noisy appearance of the spectrum, there is still a strong peak near 3.4 Hz.

Several experimental phase portraits are shown in Fig. 7. In each case x and $\dot{x}$ are determined experimentally from the

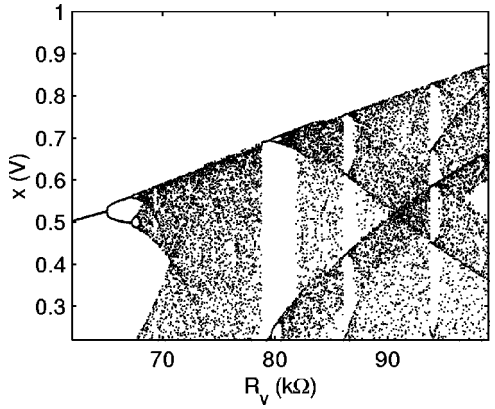

Fig. 5. An expanded view of part of the experimental bifurcation plot shown in Fig. 4.

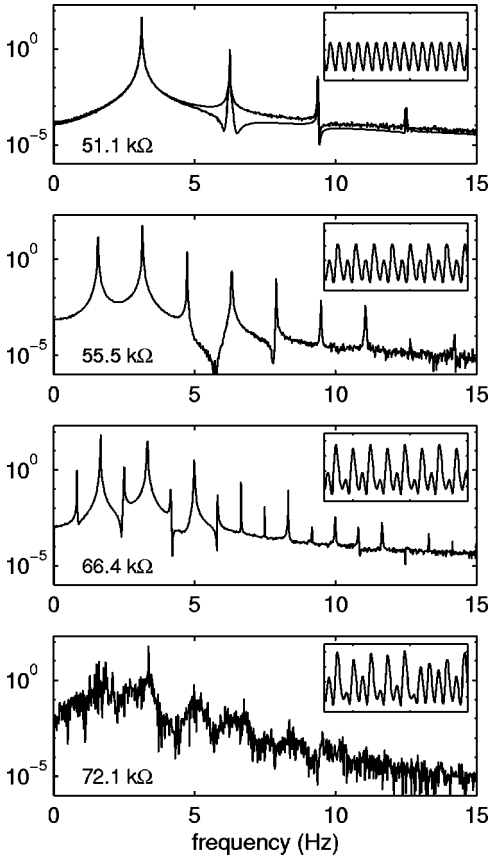

Fig. 6. Experimental power spectral density plots showing the period-doubling route to chaos as R_v is increased. The value of R_v is indicated in the lower left corner. The inset in each plot shows a sample of the experimental time series data used to generate the corresponding spectral density. The smoother line in the period-one plot shows the theoretical spectral density.

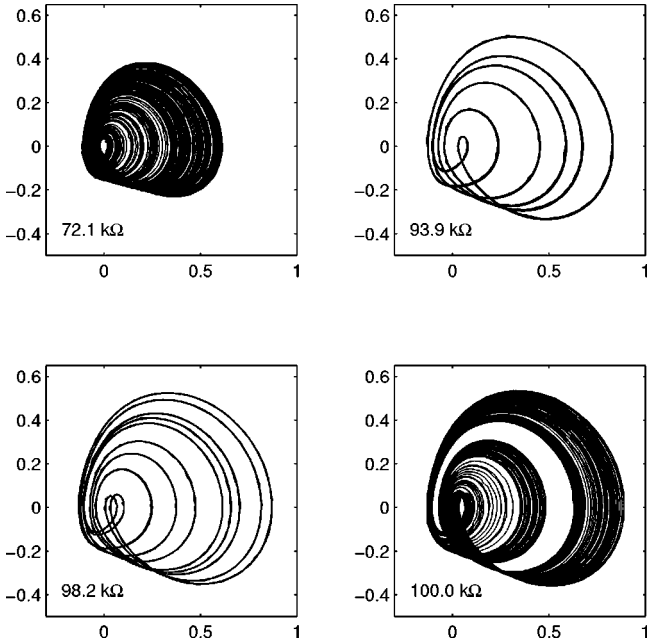

Fig. 7. Experimental phase portraits for several different values of the variable resistance R_v. In each plot x and $\dot{x}$ are plotted (in volts) on the horizontal and vertical axes, respectively. A theoretical curve is superimposed on the period-six case for comparison, although the curve is not distinguishable from the experimental curve. The period-10 attractor comes from a narrow window that is barely discernible at the far right edge of Fig. 5.

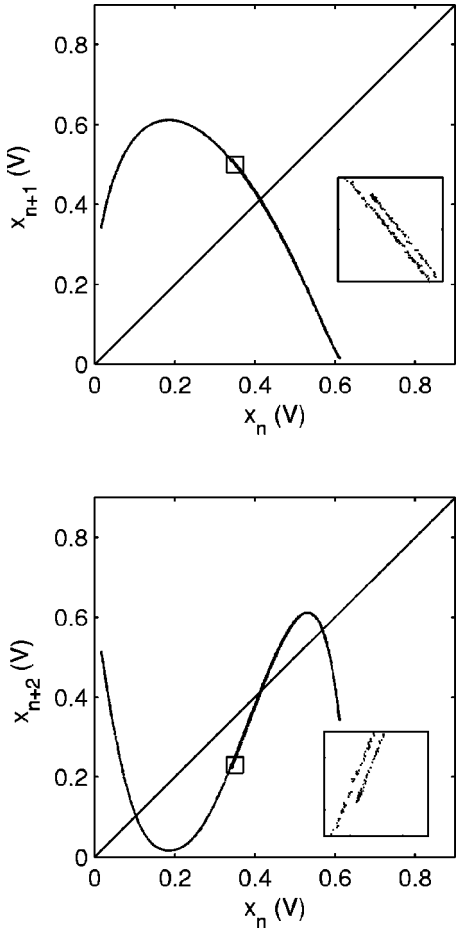

Fig. 9. First- and second-return maps for $R_v = 72.1\ \mathrm{k}\Omega$, taken from experimental data. The insets are magnified by a factor of approximately 6.5 and show the fractal structure of the plots. The intersections of the return maps with the diagonal lines give evidence for (unstable) period-one and -two orbits in the data sets. Such orbits do indeed exist, as seen in Fig. 10.

appropriate nodes in the circuit. The upper-left and lower-right plots show two different chaotic attractors. The latter is a two-banded attractor taken from the region just to the left of the final bifurcation out of chaos in Fig. 4. The upper-right and lower-left plots show period-six and -10 attractors, which are taken from relatively narrow windows of periodicity discernible in Figs. 4 and 5. A theoretical curve is superimposed on the period-six attractor, but is not distinguishable due to the excellent agreement. Comparisons between theoretical and experimental phase portraits for several periodic attractors show agreement typically within 3–6 mV, with the agreement being somewhat worse for larger values of R_v. For $R_v = 123.2\ \mathrm{k}\Omega$ (near the bifurcation from period-four to period-two) the theoretical and experimental attractors differ by up to about 8 mV. Figure 8 shows a stereoscopic plot of the first 2000 points of one of the chaotic attractors in Fig. 7.

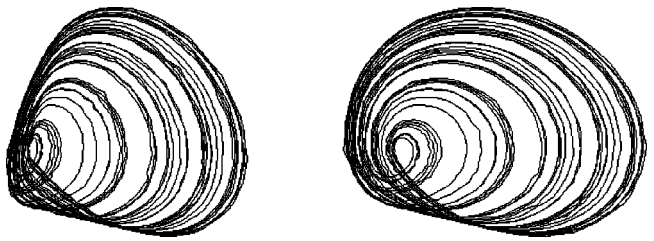

Fig. 8. Stereoscopic plot of the chaotic attractor at $R_v = 72.1\ \mathrm{k}\Omega$. The x and $\dot{x}$ coordinates are taken from experimental data. The third coordinate is proportional to $\ddot{x}$ and is determined numerically by using pairs of $\dot{x}$ values.

C. Case study of a chaotic attractor

In this section we focus our attention on the chaotic attractor near $R_v = 72.1\ \mathrm{k}\Omega$. Phase portraits for this attractor are shown in Figs. 7 and 8. One point of comparison between theory and experiment for this case is provided by the return map associated with the attractor. To construct a return map for a time-continuous system, we first construct an array containing successive maxima x_n. The r-return map is then a plot of x_{n+r} versus x_n. For a system such as ours, the return maps have a fractal structure. Figure 9 shows experimental plots of the first- and second-return maps for $R_v = 72.1\ \mathrm{k}\Omega$. The inset in each case shows the first splitting of the return map associated with its fractal structure. Subsequent splittings at higher magnification are not observable experimentally due to noise in the experimental data. A comparison with the theoretical first-return map shows quite good agreement, with the theoretical values typically being larger than the experimental ones by 2–4 mV. The disagreement is due in part to the fact that our fitting procedure for determining experimental maxima tends to underestimate the maxima slightly. The theoretical first-return map shows further fractal structure. For example, a numerical solution with step size 0.015 625 ms reveals that the main inverted parabola of the return map is actually two separate lines, sepa-

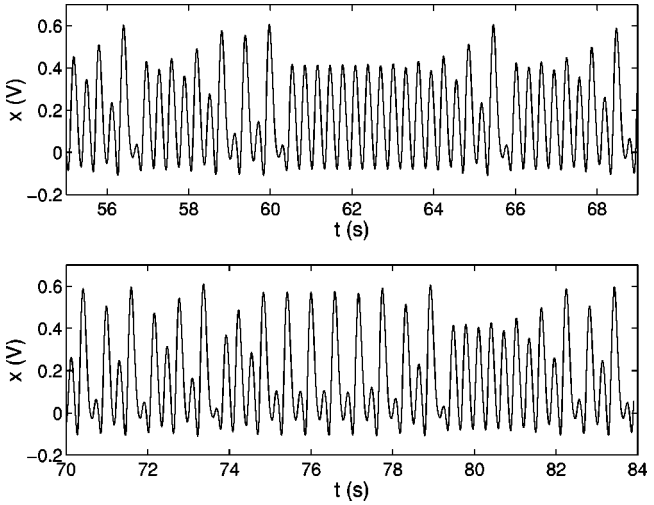

Fig. 10. Experimental wave forms showing unstable period-one and -two orbits within the chaotic time series data for $R_v = 72.1\ \mathrm{k}\Omega$. The top plot shows an unstable period-one orbit starting shortly after $t = 60$ s, with a maximum near 0.41 V. The bottom plot shows an unstable period-two orbit starting just before $t = 75$ s, with maxima near 0.57 V and 0.10 V. The plots themselves are taken from different datasets.

rated by about 0.026 mV at the peak (further splitting of these lines is not evident with this step size). The experimental noise at the peak has a width of about 1 mV, explaining why the splitting is not observed experimentally.

Return maps can be used to study periodic orbits within the data set.[34,35] A diagonal line is superimposed on each of the plots in Fig. 9. In the top plot the diagonal intersects the first-return map near $x_n \simeq 0.41$ V, giving evidence for a period-one orbit within the data set. Because the magnitude of the slope of the return map is greater than unity at that point, the period-one orbit is unstable.[36] A search through the experimental time series data does indeed yield unstable period-one orbits within the chaotic oscillations. The top plot in Fig. 10 shows such an example. In this case the unstable period-one behavior persists for approximately 10 oscillations (which is longer than typical for such orbits in the data set). As expected, the maxima of the oscillations occur at approximately 0.41 V. In a similar way, the intersection of the diagonal line with the second-return map in Fig. 9 gives evidence for unstable period-two orbits with maxima at approximately 0.57 V and 0.10 V. Examination of the time series data again yields such orbits, as shown in Fig. 10.

Another point of comparison between theory and experiment is the largest Lyapunov exponent, which measures the average exponential rate of spreading of nearby trajectories and is positive for a chaotic system. The experimental value of this exponent is estimated using the method of Wolf *et al.*[37] as implemented in the Chaos Data Analyzer program.[38] The time series consists of 3228 points sampled at the local maximum of each cycle for the case shown in Fig. 9. Candidate pairs are chosen assuming a noise floor of 0.1% and followed for one cycle. The resulting largest Lyapunov exponent (base e) is estimated to be $1.34 \pm 0.08\ \mathrm{s}^{-1}$. By comparison, iterating the theoretical expression in Eqs. (6) and (9) (modified slightly to use the measured component values) gives a spectrum of exponents[39] $(1.269, 0, -15.037) \pm 0.001\ \mathrm{s}^{-1}$, in agreement within the estimated errors of about 6%. From these values, the Kaplan–Yorke dimension[40] is found to be $D_{\mathrm{KY}} = 2 + 1.269/15.037 \simeq 2.084$. The proximity of this value to two explains why the return map is a relatively thin fractal.

IV. DISCUSSION AND CONCLUSIONS

The circuit described in this work is modeled very accurately by a simple, third-order differential equation whose solutions display a rich variety of chaotic and periodic behavior. Investigation of the circuit yields excellent agreement between theory and experiment for quantities such as power spectra, bifurcation points, phase portraits, and Lyapunov exponents. For some of these quantities the agreement is within 1%. The quality of this agreement and the stability of the circuit itself give the circuit great potential as a serious research tool for studies of synchronization, chaos control, higher-dimensional chaos, and other topics within nonlinear dynamics.

Investigation of the circuit is very accessible to undergraduates and is particularly well suited as a research project for junior- or senior-level students. The range of projects associated with the system need only be limited by the students' imaginations. A detailed investigation may be undertaken using commercially available A/D systems, or, at a somewhat less sophisticated level, the data may be digitized using a digital oscilloscope. Several options for investigation also are available without digitizing the data. For example, the $X-Y$ setting on an oscilloscope may be used to display phase portraits in real time. The circuit also may be simplified by substituting an analog potentiometer for the digital ones that we use.

Students will invariably be fascinated as they observe the changes in behavior as R_v is varied. Other variations on the circuit are also possible. For example, different nonlinearities $D(x)$ may be substituted in place of the one used here.[16,17] Furthermore, the operating frequency of the circuit (approximately $1/(2\pi RC)$) may easily be scaled by using different resistors or capacitors than those that we used. Scaling the frequency to the audio range and connecting the output to a speaker allows for an audible demonstration of chaos, with clearly distinguishable period doublings (frequency halvings) en route to chaos.[15] On the theoretical side, modeling the behavior of the circuit serves as an excellent review of differential equations for students. They might write their own programs to solve the equations or use software such as Matlab or Mathematica to do this. The circuit offers many possibilities for theoretical and experimental investigation, ranging from simple qualitative demonstrations to indepth analyses, making it ideal for use in an undergraduate setting.

ACKNOWLEDGMENTS

We thank J. Goldberg, W. Holmes, H. Voss, S. Brandle, T. Klein, J. Kolb, S. Price, K. Knapp, D. Simons, J. Oehrig, and J. Schea for valuable assistance at various stages of this work. K.K. was supported by an award from Research Corporation during early stages of this work.

[a]Electronic mail: knkiers@tayloru.edu
[b]Electronic mail: Dory_Schmidt/rad@di.mdacc.tmc.edu
[c]Electronic mail: sprott@physics.wisc.edu

[1]T. Mishina, T. Kohmoto, and T. Hashi, "Simple electronic circuit for the demonstration of chaotic phenomena," Am. J. Phys. **53**, 332–334 (1985).
[2]K. Briggs, "Simple experiments in chaotic dynamics," Am. J. Phys. **55**, 1083–1089 (1987).

[3]R. Zimmerman, S. Celaschi, and L. G. Neto, "The electronic bouncing ball," Am. J. Phys. **60**, 370–375 (1992).
[4]T. Mitchell and P. B. Siegel, "A simple setup to observe attractors in phase space," Am. J. Phys. **61**, 855–856 (1993).
[5]M. T. Levinsen, "The chaotic oscilloscope," Am. J. Phys. **61**, 155–165 (1993).
[6]B. K. Clark, R. F. Martin, Jr., R. J. Moore, and K. E. Jesse, "Fractal dimension of the strange attractor of the bouncing ball circuit," Am. J. Phys. **63**, 157–163 (1995).
[7]B. K. Jones and G. Trefan, "The Duffing oscillator: A precise electronic analog chaos demonstrator for the undergraduate laboratory," Am. J. Phys. **69**, 464–469 (2001).
[8]P. K. Roy and A. Basuray, "A high frequency chaotic signal generator: A demonstration experiment," Am. J. Phys. **71**, 34–37 (2003).
[9]T. Matsumoto, L. O. Chua, and M. Komuro, "The double scroll," IEEE Trans. Circuits Syst. **32**, 797–818 (1985).
[10]T. Matsumoto, L. O. Chua, and M. Komuro, "Birth and death of the double scroll," Physica D **24**, 97–124 (1987).
[11]G. Chen and T. Ueta, editors, *Chaos in Circuits and Systems* (World Scientific, London, 2002).
[12]T. P. Weldon, "An inductorless double scroll chaotic circuit," Am. J. Phys. **58**, 936–941 (1990).
[13]A. S. Elwakil and M. P. Kennedy, "Generic RC realizations of Chua's circuit," Int. J. Bifurcation Chaos Appl. Sci. Eng. **10**, 1981–1985 (2000).
[14]A. S. Elwakil and M. P. Kennedy, "Construction of classes of circuit-independent chaotic oscillators using passive-only nonlinear devices," IEEE Trans. Circuits Syst., I: Fundam. Theory Appl. **48**, 289–307 (2001).
[15]J. C. Sprott, "Simple chaotic systems and circuits," Am. J. Phys. **68**, 758–763 (2000).
[16]J. C. Sprott, "A new class of chaotic circuit," Phys. Lett. A **266**, 19–23 (2000).
[17]K. Kiers, T. Klein, J. Kolb, S. Price, and J. C. Sprott, "Chaos in a nonlinear analog computer," Int. J Bifurcations Chaos (to be published).
[18]H. P. W. Gottlieb, "Question #38. What is the simplest jerk function that gives chaos?," Am. J. Phys. **64**, 525 (1996).
[19]S. J. Linz, "Nonlinear dynamical models and jerky motion," Am. J. Phys. **65**, 523–526 (1997).
[20]J. C. Sprott, "Some simple chaotic jerk functions," Am. J. Phys. **65**, 537–543 (1997).
[21]S. J. Linz and J. C. Sprott, "Elementary chaotic flow," Phys. Lett. A **259**, 240–245 (1999).
[22]J. C. Sprott and S. J. Linz, "Algebraically simple chaotic flows," Int. J. Chaos Theory Appl. **5**, 3–22 (2000).
[23]E.-W. Bai, K. E. Lonngren, and J. C. Sprott, "On the synchronization of a class of electronic circuits that exhibit chaos," Chaos, Solitons Fractals **13**, 1515–1521 (2002).
[24]K. M. Cuomo and A. V. Oppenheim, "Circuit implementation of synchronized chaos with applications to communications," Phys. Rev. Lett. **71**, 65–68 (1993).
[25]The circuit also differs from that in Ref. 15 in a few other respects. For example, the present circuit does not use a passive integrator.
[26]For the particular circuit that we study only the combination V_0R/R_0 is relevant, and it only affects the amplitude of the signal (as long as the op amps do not saturate). Thus V_0 cannot be used as a control parameter for this circuit. Such is not necessarily the case if different nonlinearities are employed.
[27]P. Horowitz and W. Hill, *The Art of Electronics*, 2nd ed. (Cambridge University Press, New York, 1989).
[28]Note that because the output of an integrator is the integral of its input, its input is also the derivative of its output.
[29]Note that this expression assumes that zero current leaves the output, a situation that holds more rigorously if the output is followed by a voltage follower amplifier. We do not use a voltage follower in the experiment. As a result, Eq. (8) is slightly altered once the subcircuit is inserted into the circuit itself, with the factor $1/R_2$ on the left-hand side replaced by $1/R_2 + 1/R$. The approximation quoted in Eq. (9) is not affected by this change.
[30]In a detailed study of the simpler single-diode circuit of Ref. 15, we employed a piecewise fit of the diode's $I-V$ curve (using several values of α and I_S). Even with the careful fit to the $I-V$ curve, the agreement between theoretical and experimental bifurcation points was not as good as in the present case, and the theoretical and experimental bifurcation diagrams contained some noticeable qualitative differences.
[31]http://www.css.tayloru.edu/~knkiers
[32]Note that the data set is AC-coupled before the FFT to eliminate a strong peak near zero Hz.
[33]One might expect the theoretical curve to contain a series of delta functions. The finite sample size (8192 points) leads to the observed nonzero widths of the peaks in this curve.
[34]D. P. Lathrop and E. J. Kostelich, "Characterization of an experimental strange attractor by periodic orbits," Phys. Rev. A **40**, 4028–4031 (1989).
[35]C. Flynn and N. Wilson, "A simple method for controlling chaos," Am. J. Phys. **66**, 730–735 (1998).
[36]E. Ott, *Chaos in Dynamical Systems* (Cambridge University Press, New York, 1993).
[37]A. Wolf, J. B. Swift, H. L. Swinney, and J. A. Vastano, "Determining Lyapunov exponents from a time series," Physica D **16**, 285–317 (1985).
[38]J. C. Sprott and G. Rowlands, *Chaos Data Analyzer: The Professional Version* (Physics Academic Software, Raleigh, NC, 1995).
[39]J. C. Sprott, *Chaos and Time-Series Analysis* (Oxford University Press, Oxford, 2003).
[40]J. Kaplan and J. Yorke, in *Lecture Notes in Mathematics*, edited by H.-O. Peitgen and H.-O. Walther (Springer, Berlin, 1979), Vol. 370, pp. 228–237.